# HAWT Blade CFD Simulation


January 22, 2026

**Team Members:**

| | |
|---|---|
| Walid Sherif | 202200702 |
| Abdelrhman Alnaqeeb | 202200281 |
| Marwan Amr | 202200050 |
| Abdelrhman Ibrahim | 202200224 |

**Supervisors:**

Dr. Mohamed Abdelnaby
Eng. Asmaa AlaaElDeen

**Institution:**

Zewail City for Science and Technology

# Contents

# 1 Problem Description

## 1.1 Project Overview

This project entails a comprehensive Computer-Aided Engineering (CAE) analysis of a Horizontal Axis Wind Turbine (HAWT) blade. Building upon the blade geometry designed in Assignment 3, this study integrates Computational Fluid Dynamics (CFD) and Finite Element Analysis (FEA) to evaluate the blade's performance under realistic operational scenarios.

The primary objective is to assess the aerodynamic efficiency, structural integrity, and dynamic stability of the blade. The blade geometry is constructed using the **NACA 2424** airfoil profile. The simulation process allows for the prediction of power generation capabilities and the identification of potential failure modes due to aerodynamic loading or resonance.

## 1.2 Analysis Scope

The project is divided into three distinct but interconnected analysis stages:

1. **Aerodynamic Analysis (CFD):** A 3D steady-state simulation is performed to resolve the flow field around the NACA 2424 blade. Key performance indicators such as lift, drag, torque, and the power coefficient ($C_p$) are computed.
2. **Fluid-Structure Interaction (FSI):** The pressure loads derived from the CFD analysis are mapped onto the structural model of the blade to evaluate stresses and deformation. The blade is treated as a solid wood body.
3. **Modal Analysis:** A dynamic analysis is conducted to determine the blade's natural frequencies and mode shapes. These are compared against the operational rotational frequency to assess the risk of resonance.

# 2 Used Boundary Conditions

To accurately simulate the physical environment of the wind turbine, specific boundary conditions and operational parameters were applied across the fluid and structural domains.

## 2.1 CFD Boundary Conditions

The aerodynamic simulation was set up as a steady-state analysis. A rotating reference frame (or moving mesh) approach was utilized to simulate the rotation of the blade. The domain boundaries were defined as shown in Table 1.

**Table 1:** Boundary Conditions for 3D Steady CFD Analysis

| Zone/Boundary | Type | Value / Setting |
|---|---|---|
| Inlet | Velocity Inlet | $9\,\mathrm{m\,s^{-1}}$ (Axial Flow) |
| Outlet | Pressure Outlet | 0 Pa (Gauge Pressure) |
| Blade Surface | Wall | No Slip Condition |
| Far Field | Wall | Free Slip / Shear Free |
| Fluid Domain Motion | Rotational Velocity | 400 rpm |
| Turbulence Model | k-$\omega$ SST | Standard Wall Functions |

## 2.2 Structural (FSI) Boundary Conditions

For the structural analysis, the blade was modeled as a linear elastic material (Wood) with properties defined in the project specifications. The boundary conditions focused on constraining the blade root and applying the aerodynamic and inertial loads.

**Table 2:** Boundary Conditions for Structural and Modal Analysis

| Location/Type | Condition | Description |
|---|---|---|
| Blade Root | Fixed Support | All degrees of freedom (DOF) constrained ($U_x = U_y = U_z = 0$). |
| Blade Surface | Imported Load | Aerodynamic pressure mapped from CFD solution (FSI). |
| Global Body | Rotational Velocity | 400 rpm (Simulates centrifugal forces). |

## 2.3 Modal Analysis Setup

The modal analysis was performed using a **Pre-Stressed** setup. The static structural state (including deformation and stress stiffening from the rotation and aerodynamic loads) was used as the initial condition to calculate the natural frequencies.

- **Constraint:** Fixed Support at the Root.
- **Pre-Stress Environment:** Static Structural (FSI) Solution.
- **Material:** Wood (Density: 553.6 $\mathrm{kg\,m^{-3}}$, Young's Modulus: 89 632 MPa).

# 3 Blade Design Methodology

## 3.1 Theoretical Framework: Blade Element Momentum (BEM)

The aerodynamic design of the wind turbine blade was conducted using the Blade Element Momentum (BEM) theory. This method, as described by Chaudhary et al., combines momentum theory and blade element theory to calculate the aerodynamic forces and induction factors along the blade span.

The blade is divided into $N$ independent elements of width $dr$. The following assumptions were made during the design process:

- Each blade element is independent; there is no aerodynamic interaction between adjacent sections.
- The forces are determined solely by the lift and drag coefficients of the airfoil shape (NACA 2424).
- The flow is assumed to be steady-state.

## 3.2 Governing Equations

The local relative velocity ($v_r$) experienced by a blade element at a radial distance $r$ is a function of the free stream wind velocity ($v_0$), the rotational speed ($\omega$), and the induction factors:

$$v_r = \sqrt{[v_0(1-a)]^2 + [\omega r(1+a')]^2} \tag{1}$$

Where:

- $a$ is the axial induction factor.
- $a'$ is the tangential induction factor.

The local flow angle ($\phi_r$) determines the angle at which the wind hits the airfoil and is defined as:

$$\phi_r = \tan^{-1}\left(\frac{1-a}{(1+a')\lambda_r}\right) \tag{2}$$

Where $\lambda_r$ is the local tip speed ratio ($\lambda_r = \omega r / v_0$).

## 3.3 Prandtl's Tip Loss Correction

To account for the loss of lift near the tip of the blade due to vortex shedding, Prandtl's tip loss correction factor ($P_{tf}$) was included in the BEM calculations. This correction is essential for accurate torque prediction and is given by:

$$P_{tf} = \frac{2}{\pi}\cos^{-1}\left[\exp\left(-\frac{N_b}{2}\frac{R-r}{r\sin\phi_r}\right)\right] \tag{3}$$

Where $N_b$ is the number of blades and $R$ is the total rotor radius.

## 3.4 Optimal Geometric Parameters

To maximize power extraction, the blade geometry (twist and chord) was optimized based on the specific aerodynamic characteristics of the **NACA 2424** profile.

The optimal local twist angle ($\beta_r$) is calculated by subtracting the design angle of attack ($\alpha_d$) from the local flow angle:

$$\beta_r = \phi_r - \alpha_d \tag{4}$$

The optimal chord length distribution ($c_r$) along the span is derived to satisfy the momentum balance, incorporating the tip loss factor:

$$c_r = \frac{8\pi r P_{tf}\sin\phi_r}{N_b C_{L,d}}\left(\frac{1-\lambda_r\tan\phi_r}{\tan\phi_r + \lambda_r}\right) \tag{5}$$

Where $C_{L,d}$ is the lift coefficient of the NACA 2424 airfoil at the design angle of attack. This distribution ensures the blade operates at maximum aerodynamic efficiency along its entire length.

## 3.5 QBLADE Results

naca2424

3 blades and 0.25 [m] hub radius

Single Reynolds Number Polars

Show Blade Root Coordinates

| | Pos [m] | Chord [m] | Twist [deg] | Foil | Polar |
|---|---|---|---|---|---|
| 1 | 0.250 | 0.327 | 22.445 | NACA 2424 | NACA_2424_Re1.000_M0.00_N... 360 M |
| 2 | 0.400 | 0.221 | 12.354 | NACA 2424 | NACA_2424_Re1.000_M0.00_N... 360 M |
| 3 | 0.550 | 0.165 | 7.260 | NACA 2424 | NACA_2424_Re1.000_M0.00_N... 360 M |
| 4 | 0.600 | 0.152 | 6.092 | NACA 2424 | NACA_2424_Re1.000_M0.00_N... 360 M |
| 5 | 0.750 | 0.123 | 3.484 | NACA 2424 | NACA_2424_Re1.000_M0.00_N... 360 M |
| 6 | 0.900 | 0.103 | 1.719 | NACA 2424 | NACA_2424_Re1.000_M0.00_N... 360 M |
| 7 | 1.050 | 0.089 | 0.448 | NACA 2424 | NACA_2424_Re1.000_M0.00_N... 360 M |
| 8 | 1.200 | 0.078 | -0.511 | NACA 2424 | NACA_2424_Re1.000_M0.00_N... 360 M |
| 9 | 1.350 | 0.069 | -1.259 | NACA 2424 | NACA_2424_Re1.000_M0.00_N... 360 M |
| 10 | 1.500 | 0.062 | -1.860 | NACA 2424 | NACA_2424_Re1.000_M0.00_N... 360 M |

**Figure 1:** QBLADE geometric parameters

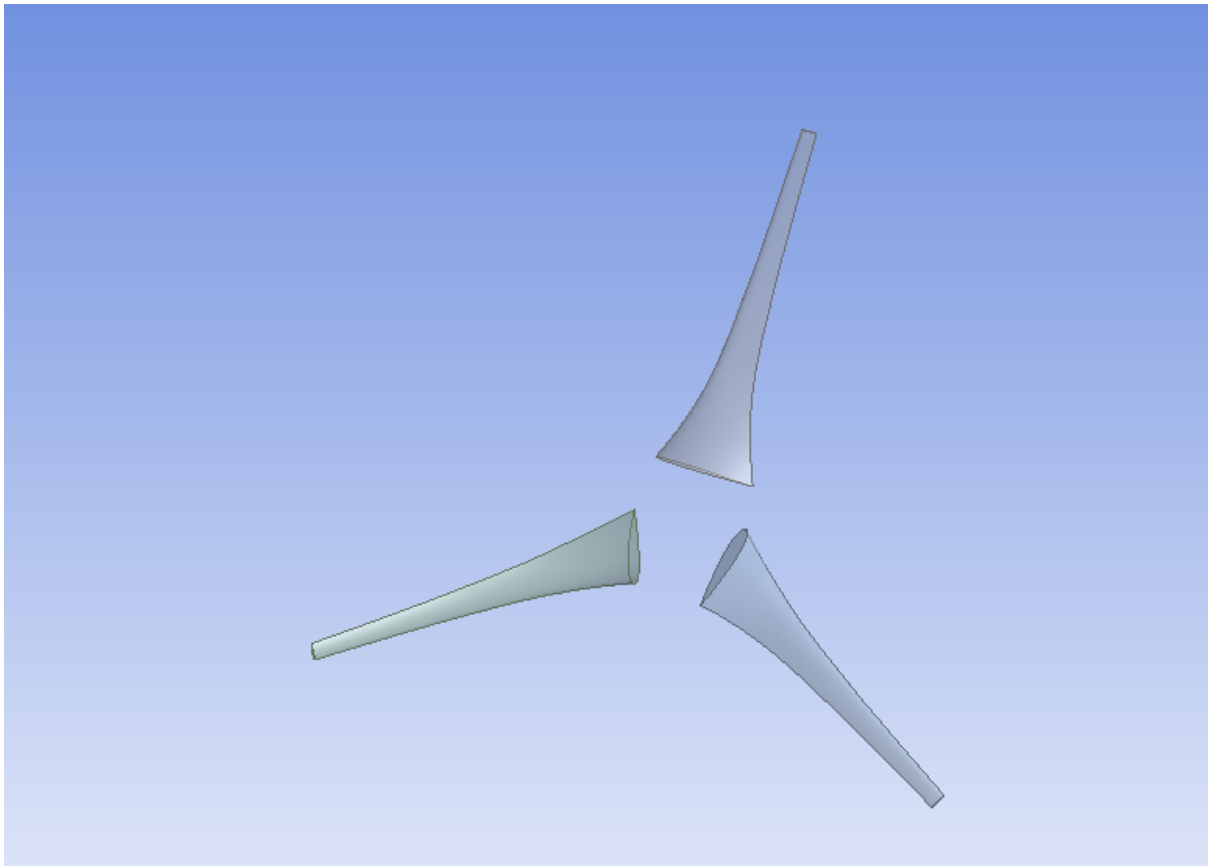

**Figure 2:** 3-Blade Rotor Geometry

# 4 Computational Mesh

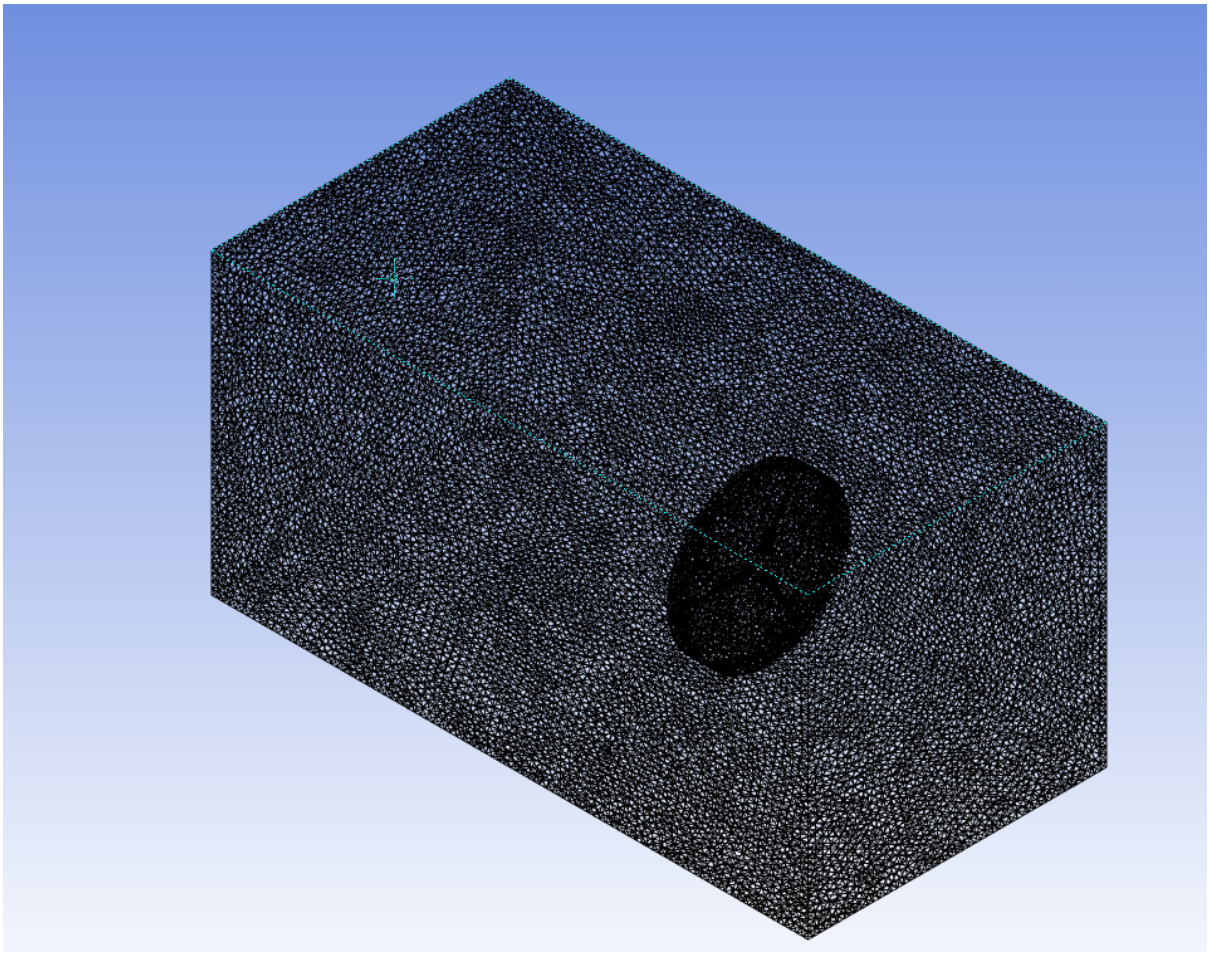

**Figure 3:** Global Mesh Domain

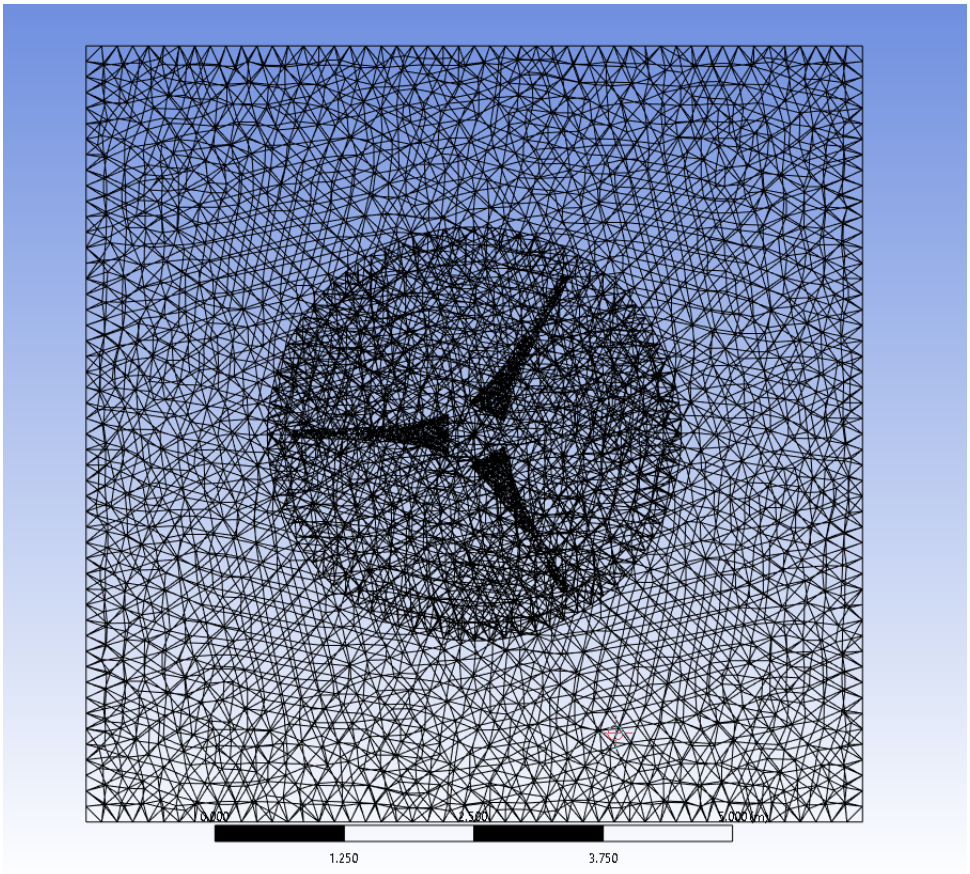


**Figure 4:** Mesh Inlet View

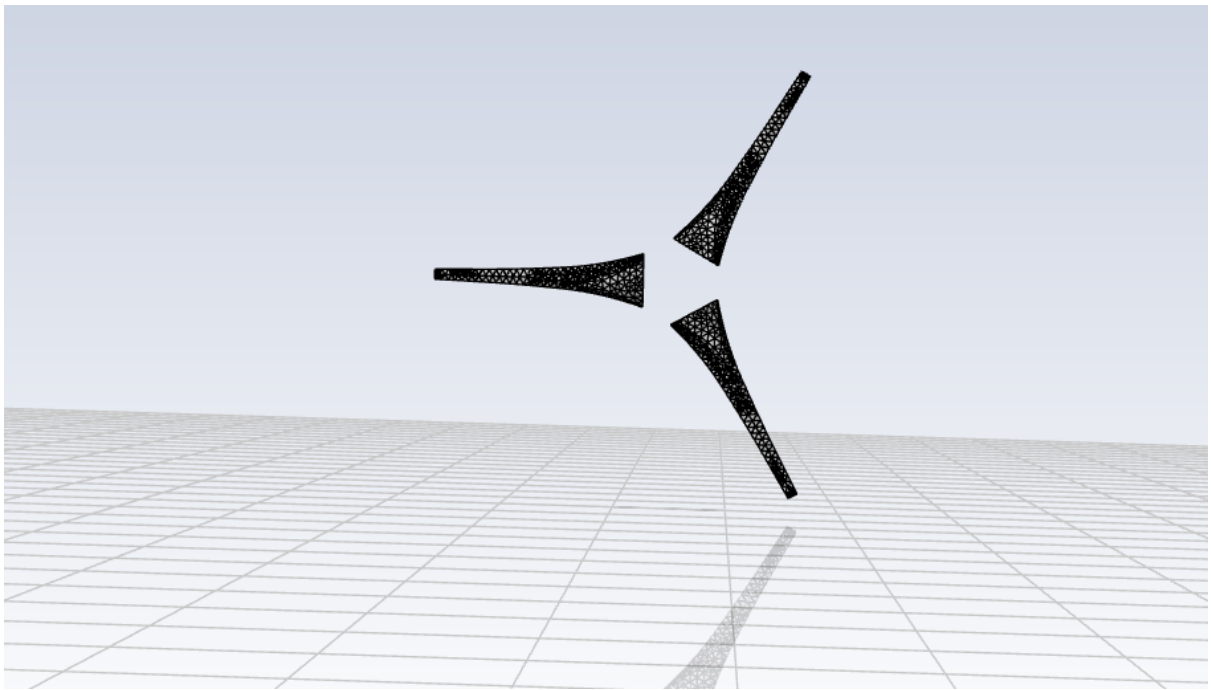

**Figure 5:** Blade Surface Mesh

# 5 CFD Results

## 5.1 Transient Analysis

### 5.1.1 Residuals and Monitors

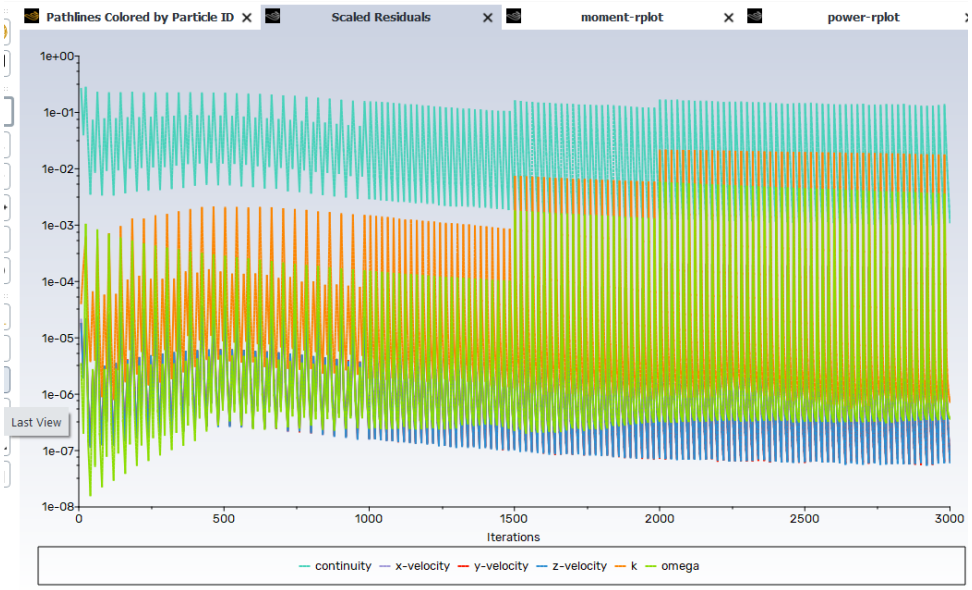


**Figure 6:** Transient Residuals

### 5.1.2 Flow Field Results

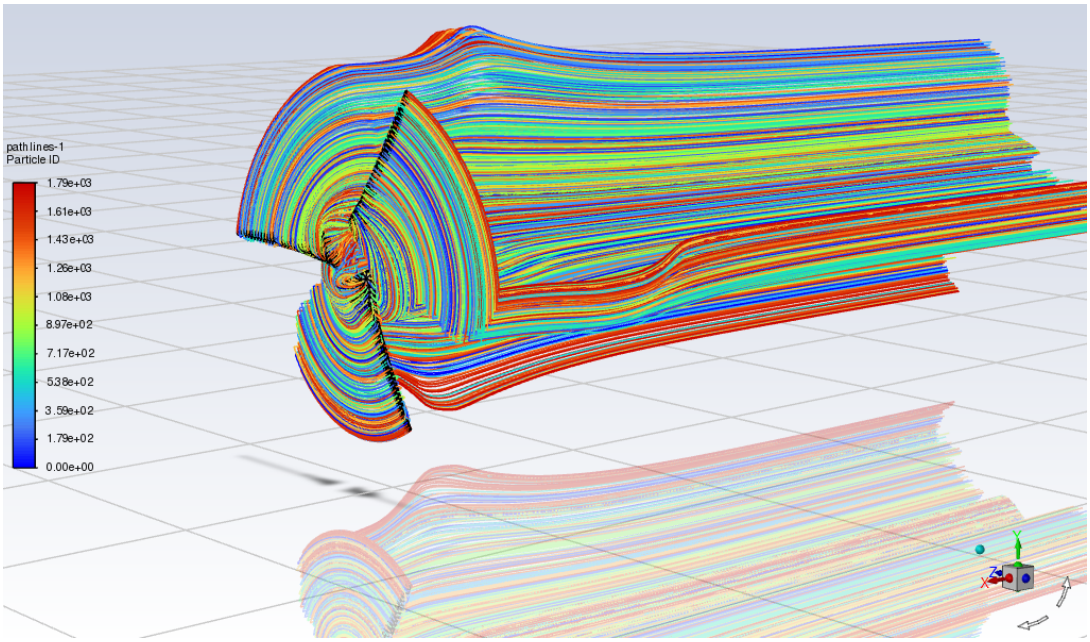


**Figure 7:** Flow Pathlines

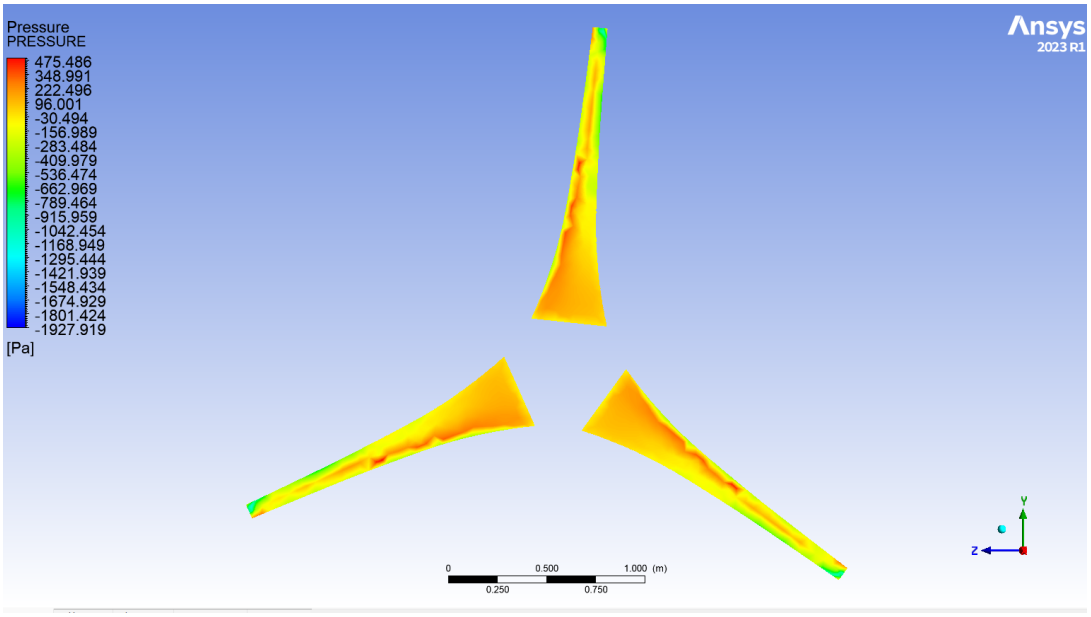


**Figure 8:** Pressure Contours (Front)

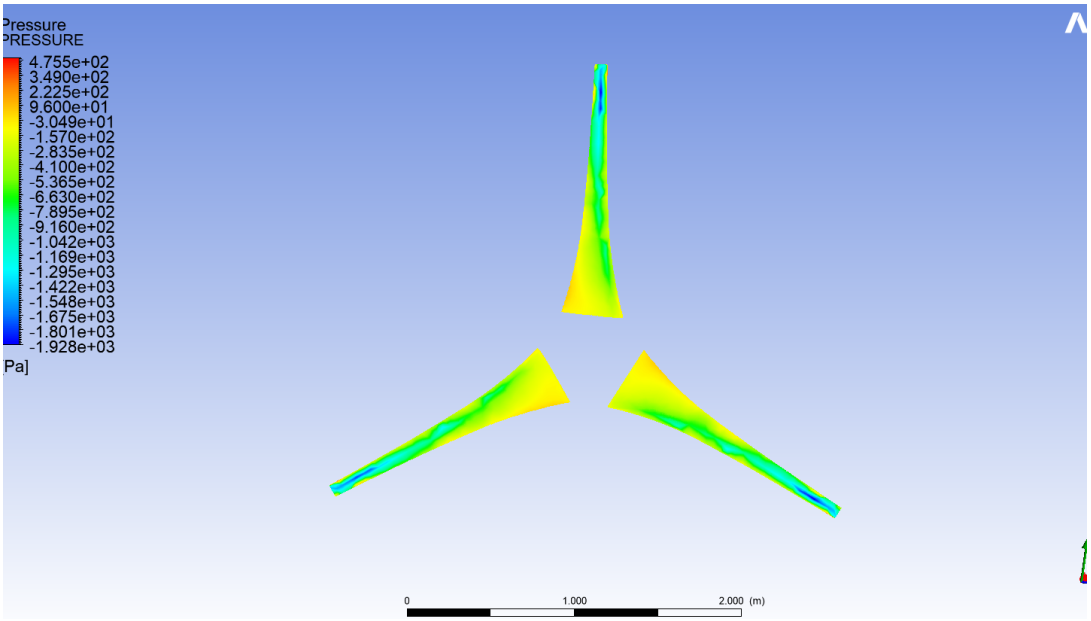


**Figure 9:** Pressure Contours (Back)

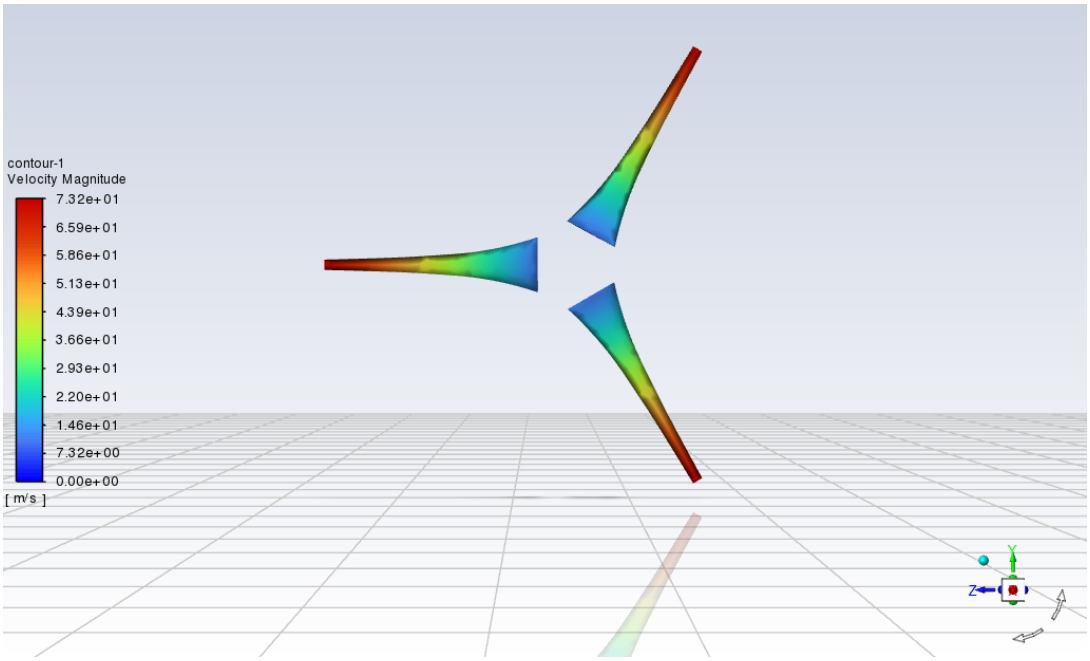


**Figure 10:** Velocity Contours

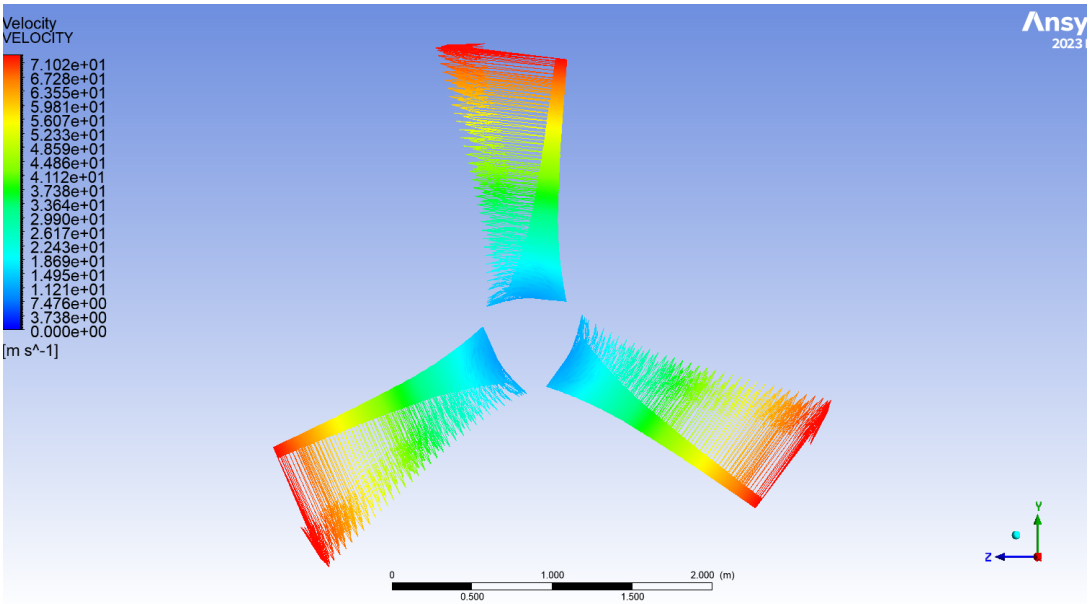


**Figure 11:** Velocity Vectors

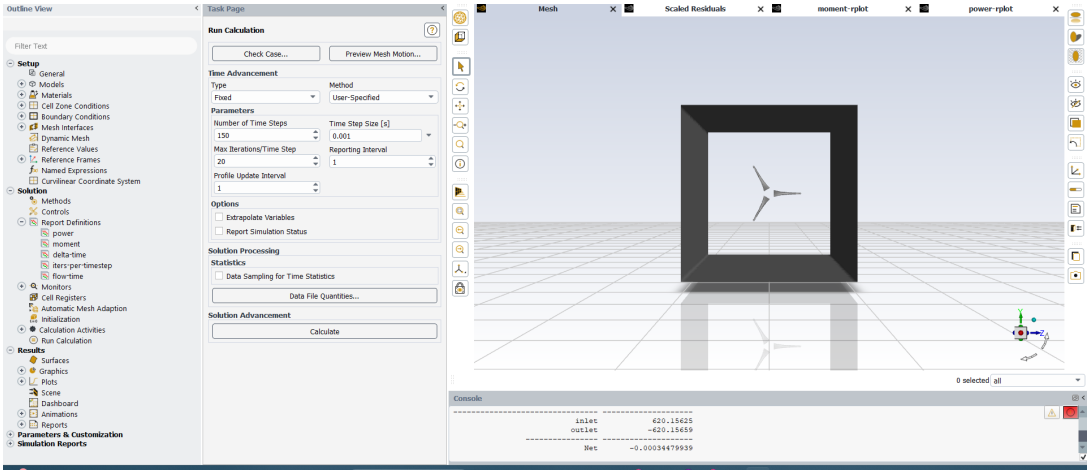


**Figure 12:** Mass Flow Rate Monitor

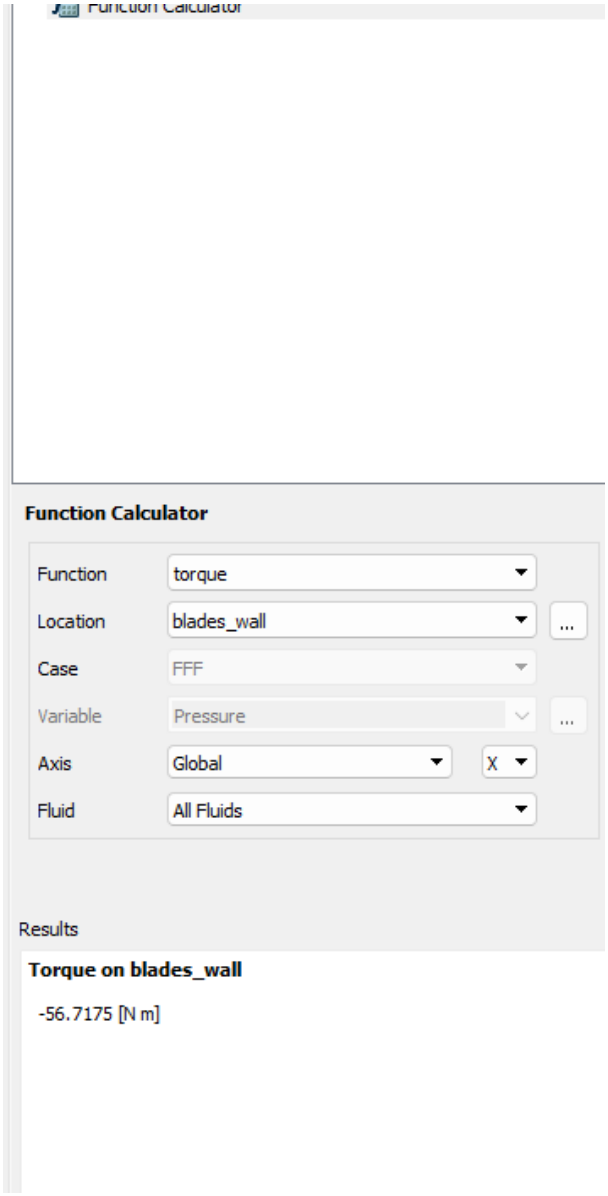


**Figure 13:** Torque Result (Transient)
**Comment**: This is wrong as it was performed in the transient analysis which contained errors. Actual correct results are in the steady study.

## 5.2 Steady-State Analysis

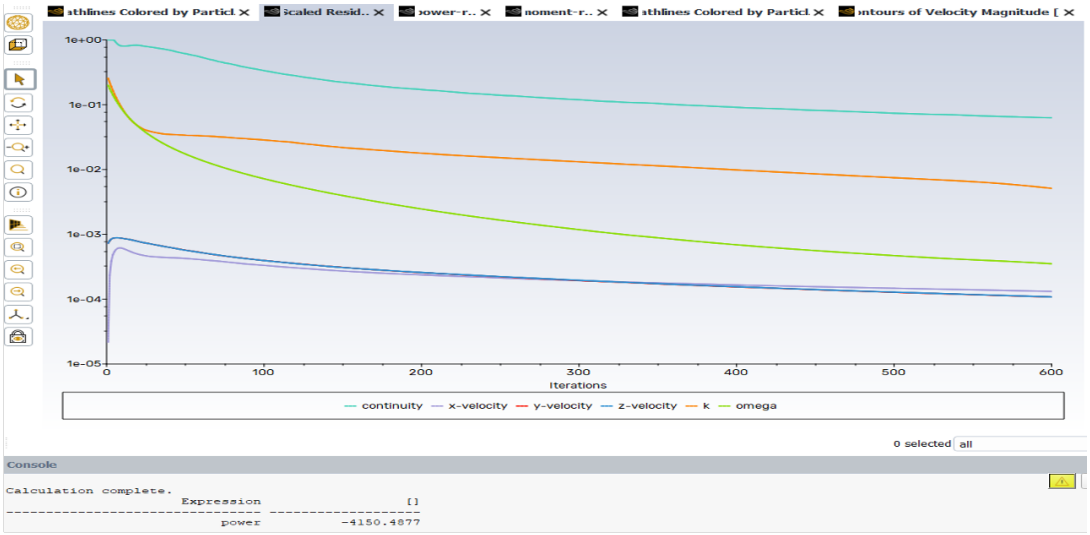


**Figure 14:** Steady-State Residuals

```
Calculation complete.

                  Mass Flow Rate              [kg/s]
-------------------------------- --------------------
                           inlet            620.15625
                          outlet           -620.15559
                 ---------------- --------------------
                             Net          0.00065723086
```

**Figure 15:** Mass Flow Rate

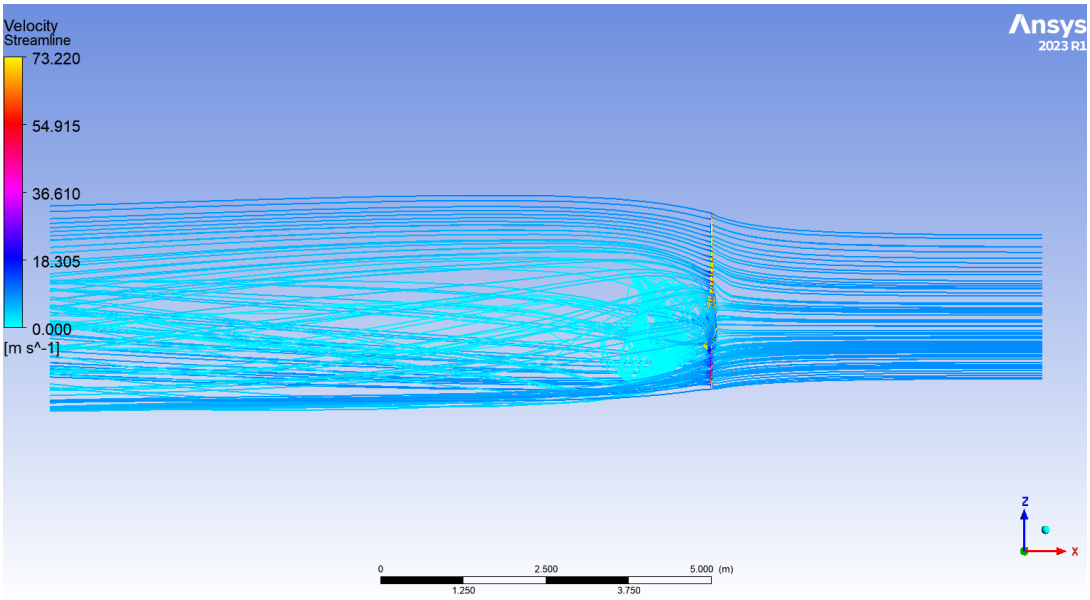


**Figure 16:** Streamlines (Steady)

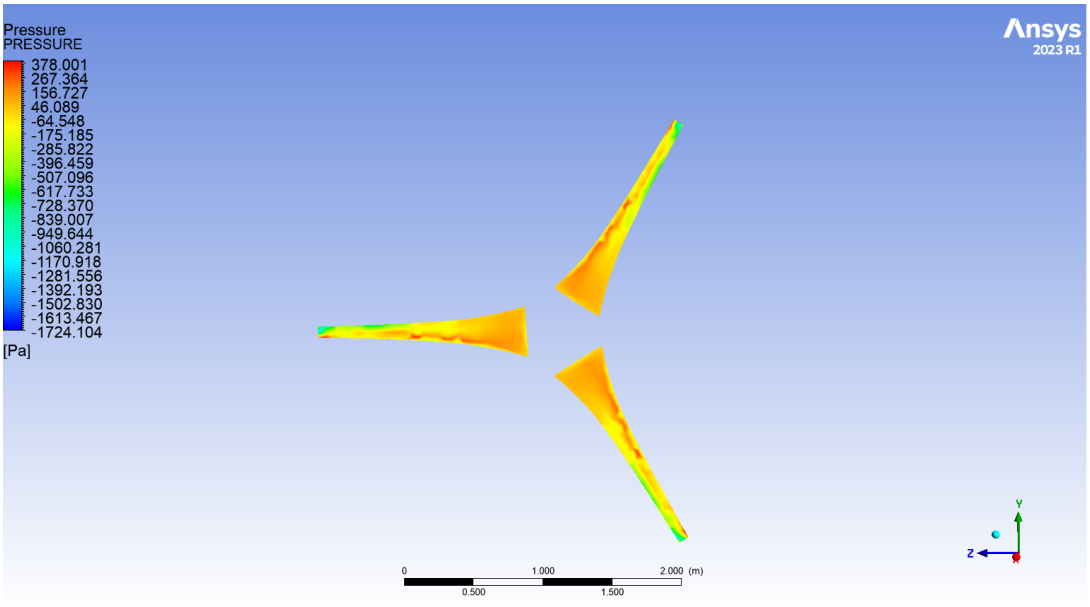


**Figure 17:** Pressure Distribution (Steady)

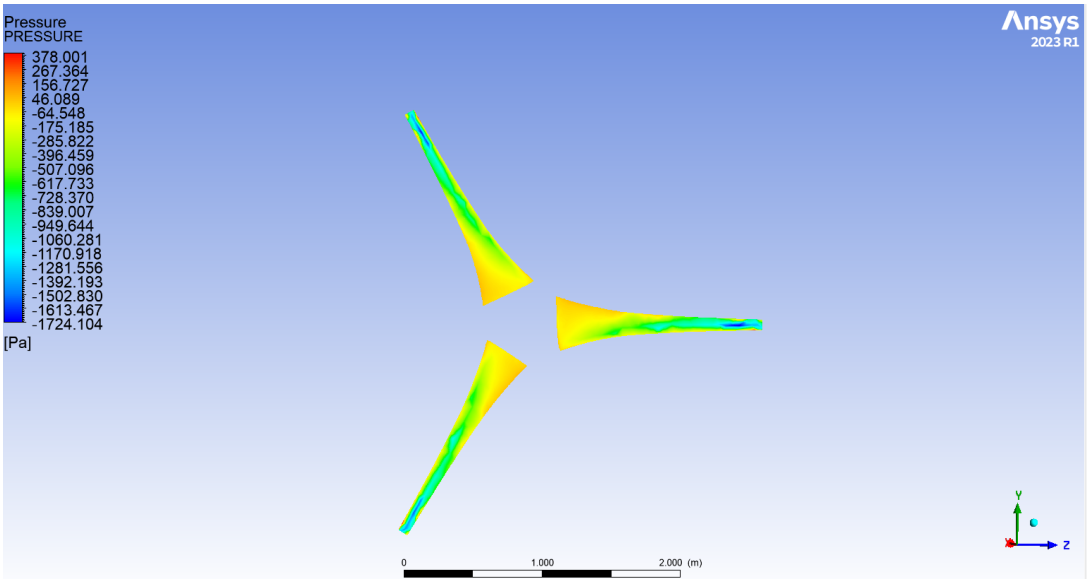


**Figure 18:** Pressure Distribution Backside (Steady)

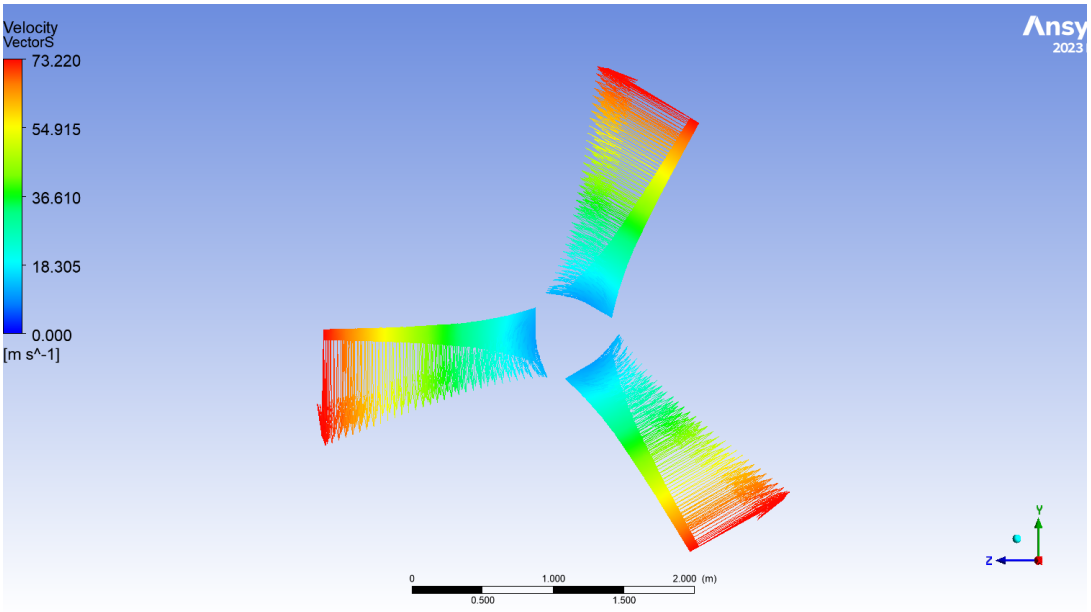


**Figure 19:** Velocity Vectors (Steady)

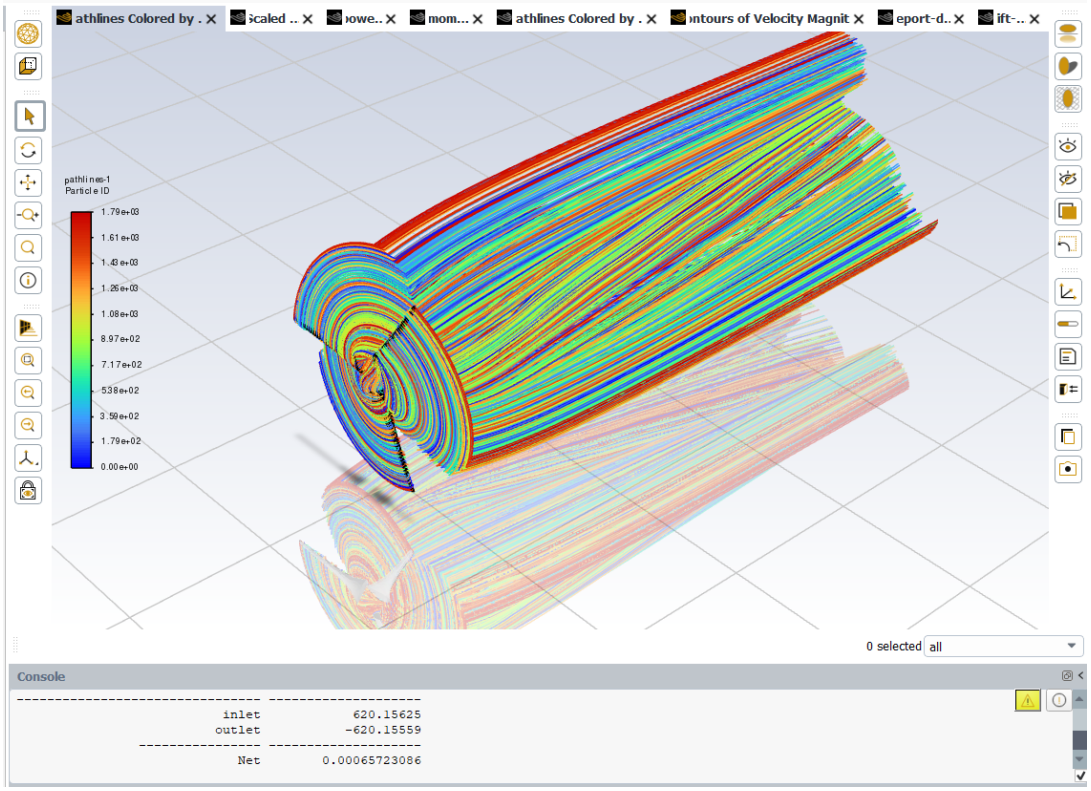


**Figure 20:** Stream Path (Steady)

The power coefficient $C_P$ is a dimensionless measure of how efficiently a wind turbine converts the available kinetic power in the wind into mechanical power on the shaft. It is defined as

$$C_P = \frac{P_{\text{turbine}}}{P_{\text{wind}}} = \frac{P_{\text{turbine}}}{\frac{1}{2}\rho A V_\infty^3},$$

where $P_{\text{turbine}}$ is the mechanical power extracted by the rotor, $\rho$ is the air density, $A = \pi R^2$ is the swept area of the rotor (with $R$ the rotor radius), and $V_\infty$ is the freestream wind speed. In practice, $P_{\text{turbine}}$ is obtained from the aerodynamic torque $T$ and rotational speed $\Omega$ via

$$P_{\text{turbine}} = T\,\Omega.$$

The theoretical upper bound for $C_P$ of an ideal, lossless actuator disk in steady, uniform flow is the Betz limit, $C_{P,\max} = 16/27 \approx 0.593$. Real turbines operate below this value due to aerodynamic, mechanical, and electrical losses, as well as practical design constraints; modern horizontal-axis wind turbines typically achieve peak $C_P$ values in the range 0.4–0.5 at their optimal tip-speed ratio.

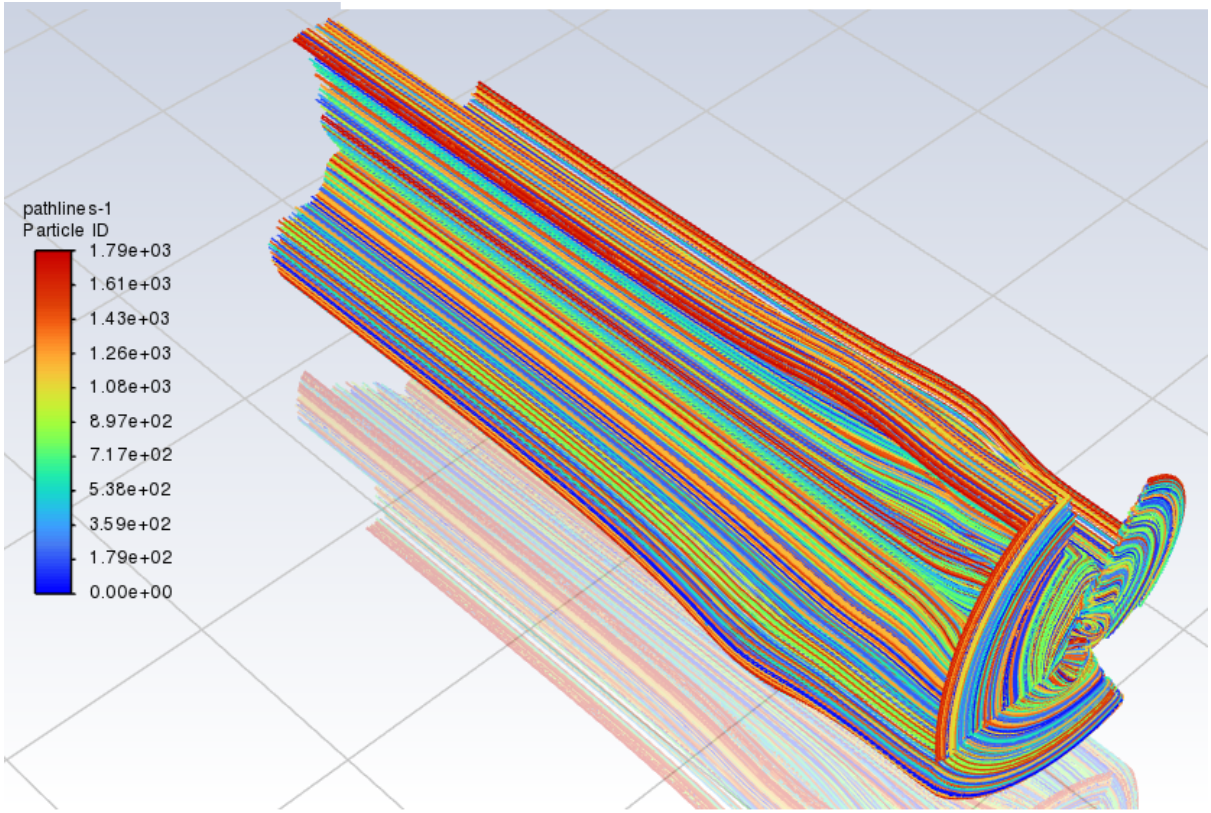


le

| | Cm |
|---|---|
| blades_wall | -25.70219 |
| Expression | [] |
| power | 1076.4077 |
| Expression | [] |
| power-coefficient-cp | 0.3410443 |

**Figure 21:** Torque, Power and Power Coefficient Result (Steady)

| Details of "Mesh" | |
|---|---|
| **Display** | |
| Display Style | Use Geometry Setting |
| **Defaults** | |
| Physics Preference | CFD |
| Solver Preference | Fluent |
| Element Order | Linear |
| Element Size | 0.15 m |
| Export Format | Standard |
| Export Preview Surface Mesh | No |
| **Sizing** | |
| **Quality** | |
| **Inflation** | |
| **Advanced** | |
| **Statistics** | |
| Nodes | 80016 |
| Elements | 411897 |
| Show Detailed Statistics | No |

**Figure 22:** mesh 1 statistics

Table of Design Points

| | A | B | C | D | E | F | G | H | I | J |
|---|---|---|---|---|---|---|---|---|---|---|
| 1 | Name | P1 - mass-flow-rate | P2 - forcex | P3 - forcey | P4 - forcez | P5 - pressure | P6 - velocity | Retain | Retained Data | Note |
| 2 | Units | kg s^-1 | N | N | N | Pa | m s^-1 | | | |
| 3 | DP 0 (Current) | 0.00097656 | -384.78 | -0.50178 | -0.56725 | -211.21 | 33.298 | ☑ | ✓ | |
| * | | | | | | | | ☐ | | |

**Figure 23:** mesh 1 parameters tracked

# 6 Grid Dependency Study Results:

| | A | B | C | D | E | F | G | H | I | J |
|---|---|---|---|---|---|---|---|---|---|---|
| 1 | Name | P1 - mass-flow-rate | P2 - forcex | P3 - forcey | P4 - forcez | P5 - pressure | P6 - velocity | Retain | Retained Data | Note |
| 2 | Units | kg s^-1 | N | N | N | Pa | m s^-1 | | | |
| 3 | DP 0 (Current) | -0.00020532 | -412.2 | 0.50355 | -1.0503 | -218.42 | 33.298 | ☑ | ✓ | |
| * | | | | | | | | ☐ | | |

**Figure 25:** mesh 2 parameters tracked

# 7 Structural Analysis (FSI)

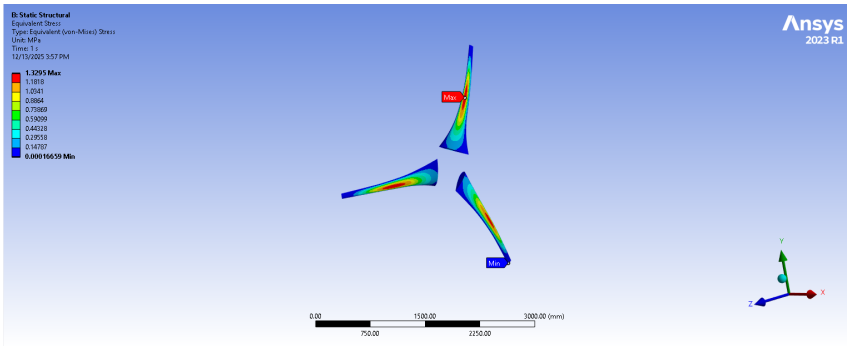


**Figure 26:** Von-Mises Stress Distribution

Details of "Mesh"

| | |
|---|---|
| **Sizing** | |
| Use Adaptive Sizing | Yes |
| Resolution | 2 |
| Mesh Defeaturing | Yes |
| Defeature Size | Default |
| Transition | Slow |
| Span Angle Center | Fine |
| Initial Size Seed | Assembly |
| Bounding Box Diagonal | 18371 mm |
| Average Surface Area | 2.6226e+007 mm² |
| Minimum Edge Length | 77.122 mm |
| **Quality** | |
| **Inflation** | |
| **Advanced** | |
| **Statistics** | |
| Nodes | 171156 |
| Elements | 881915 |
| Show Detailed Statistics | No |

**Figure 24:** mesh 1 statistics

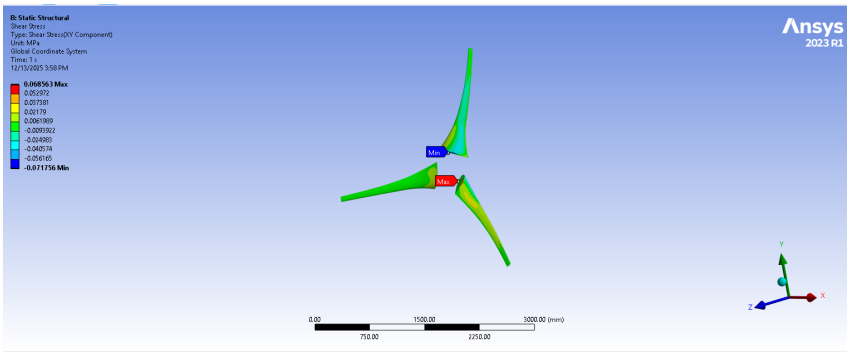


**Figure 27:** Normal Stress Distribution

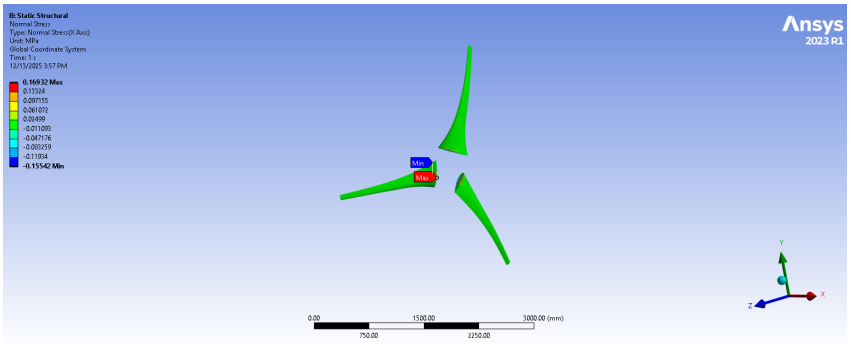


**Figure 28:** Shear Stress Distribution

# 8 Modal Analysis

## 8.1 Resonance Risk Assessment

The pre-stressed modal analysis of the NACA 2424 blade, conducted under aerodynamic loading and a rotational speed of 400 rpm, yields the first six natural frequencies at approximately 28.2 Hz, 91.3 Hz, 118.5 Hz, 214.3 Hz, 348.1 Hz, and 413.1 Hz.

To evaluate resonance risks, these natural frequencies are compared against the operational excitation frequencies:

- **Rotational Frequency (1P):** At 400 rpm, the fundamental excitation is $f_{1P} \approx 6.67$ Hz.
- **Blade Passing Frequency (3P):** For the three-bladed rotor, the dominant harmonic is $f_{3P} \approx 20.0$ Hz.

**Spectral Separation Analysis:** The fundamental natural frequency (28.2 Hz) is significantly higher than the primary excitation harmonics (1P and 3P). Consequently, the current configuration exhibits sufficient spectral separation to prevent classical resonance with the primary rotational forces during steady-state operation.
**Higher-Order Harmonic Sensitivity:** Despite the safety margin regarding the 1P and 3P orders, the first bending mode (28.2 Hz) is proximate to higher-order harmonics, specifically the 4P frequency ($\approx 26.7$ Hz). While typically less energetic, strong higher-harmonic content arising from yaw misalignment, tower-shadow effects, or turbulent inflow could potentially amplify vibrations in this mode. Furthermore, the relatively narrow separation between higher-order modes (e.g., the interval between 348 Hz and 413 Hz) suggests that the system is sensitive to physical perturbations. Localized mass or stiffness changes—such as those caused by erosion, repairs, or manufacturing tolerances—could shift these modal frequencies into operational excitation bands.

| | Mode | Frequency [Hz] |
|---|---|---|
| 1 | 1. | 28.236 |
| 2 | 2. | 28.236 |
| 3 | 3. | 28.237 |
| 4 | 4. | 91.256 |
| 5 | 5. | 91.256 |
| 6 | 6. | 91.258 |
| 7 | 7. | 118.47 |
| 8 | 8. | 118.47 |
| 9 | 9. | 118.47 |
| 10 | 10. | 214.29 |
| 11 | 11. | 214.29 |
| 12 | 12. | 214.3 |

**Figure 29:** Table of Natural Frequencies

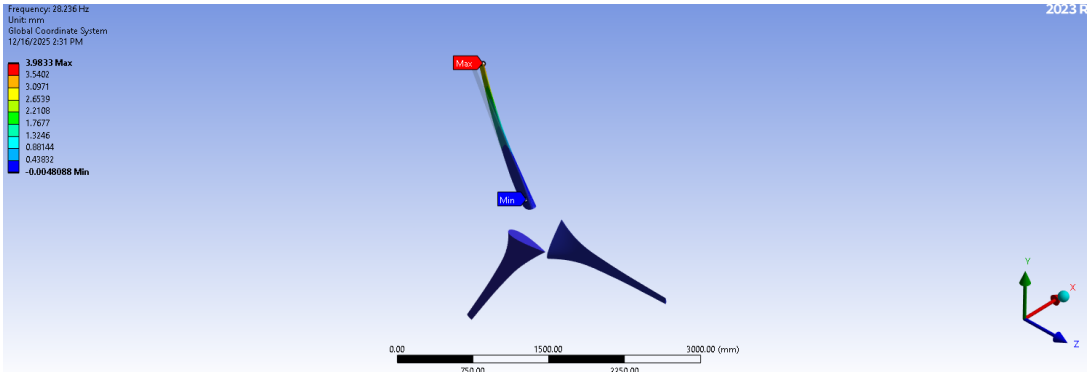


**Figure 30:** Mode Shape 1

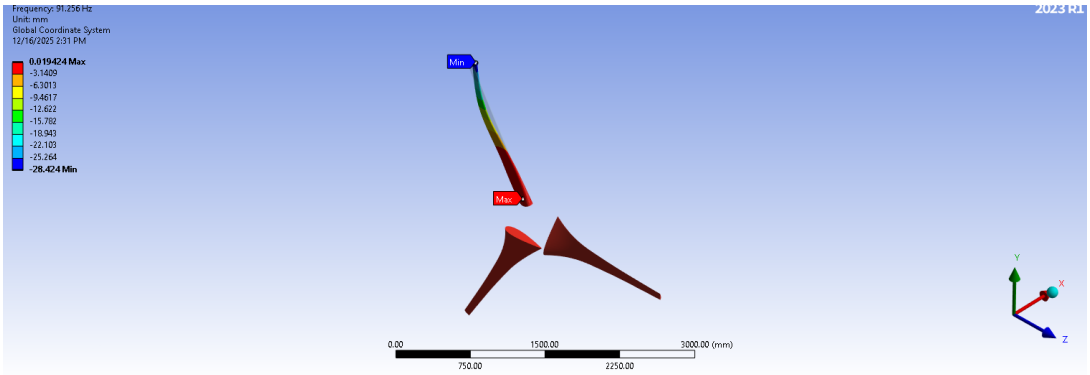


**Figure 31:** Mode Shape 2

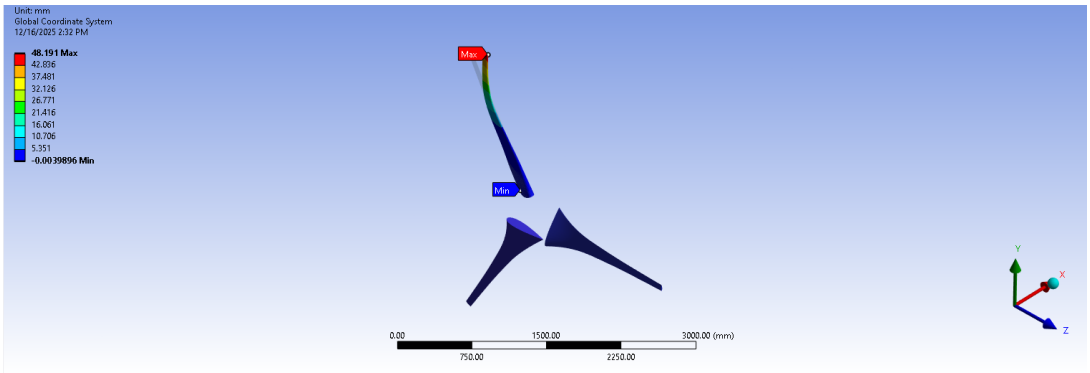


**Figure 32:** Mode Shape 3

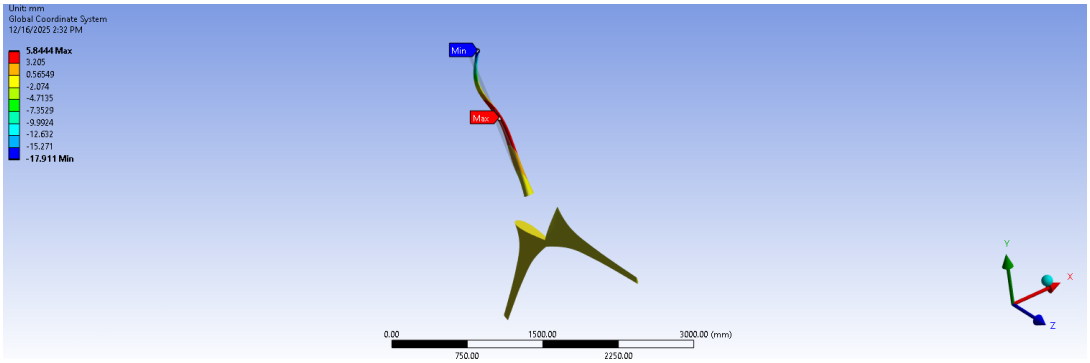


**Figure 33:** Mode Shape 4

# 9 Result Validation

This section presents a systematic comparison between the current project and two relevant literature studies to validate the adopted methodology and assess the credibility of the obtained aerodynamic results. The validation is conducted through a comparison of simulation workflows and resulting aerodynamic performance, specifically the power coefficient ($C_p$).

The benchmark studies include:

1. **Radi et al. (2024):** Evaluates HAWT performance using NACA 2424 airfoils via BEM theory.

2. **Terefa et al. (2025):** Compares BEM, QBlade, and 3D CFD for small-scale turbines.

## 9.1 Comparison of Methodological Workflows

While literature often focuses on simplified aerodynamic models, this project adopts a comprehensive **Computer-Aided Engineering (CAE)** workflow. As summarized in Table 3, our approach extends beyond basic BEM/CFD by integrating one-way Fluid-Structure Interaction (FSI) and pre-stressed modal analysis.

**Table 3:** Comparison of analysis workflows between literature and current project

| Analysis Stage | Radi et al. | Terefa et al. | Our Project |
|---|---|---|---|
| Airfoil-based design | Yes | Yes | Yes |
| BEM analysis | Yes | Yes | Yes |
| QBlade analysis | No | Yes | Yes |
| 3D CFD simulation | No | Yes | Yes |
| Torque/Power extraction | Yes | Yes | Yes |
| Structural (FSI) analysis | No | No | Yes |
| Modal analysis | No | No | Yes |
| Resonance assessment | No | No | Yes |

## 9.2 Comparison of Aerodynamic Results

**Power Coefficient Evaluation:** Radi et al. reported a maximum $C_p \approx 0.438$ using BEM theory. However, Terefa et al. demonstrated that CFD-based simulations predict lower values

($C_p \approx 0.395$) due to 3D aerodynamic losses.

In this project, a $C_p \approx 0.34$ was obtained via steady-state 3D CFD. As illustrated in Figure 35, our results follow the established trend where higher-fidelity CFD models predict more conservative (and realistic) performance than simplified BEM models.

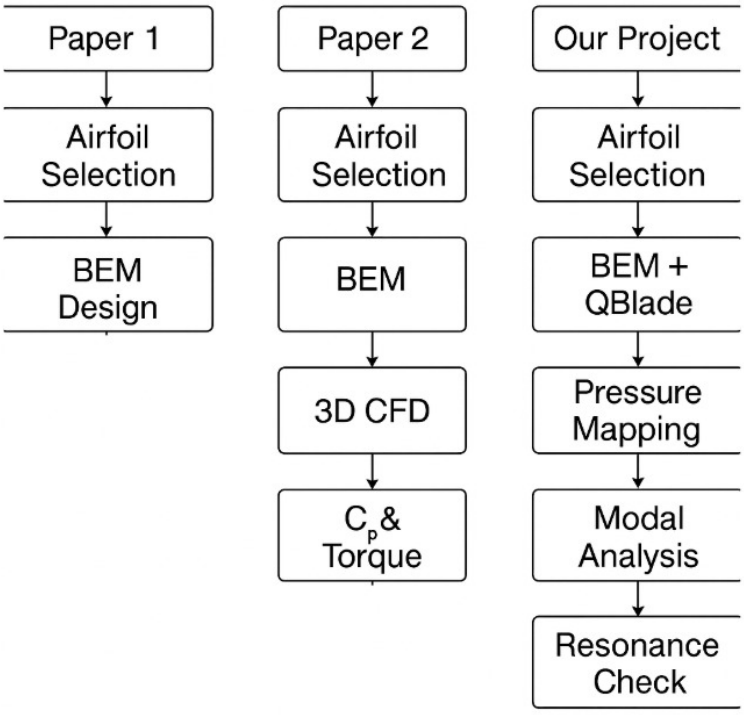


**Figure 34:** Comparison of power coefficient ($C_p$) between literature and project results

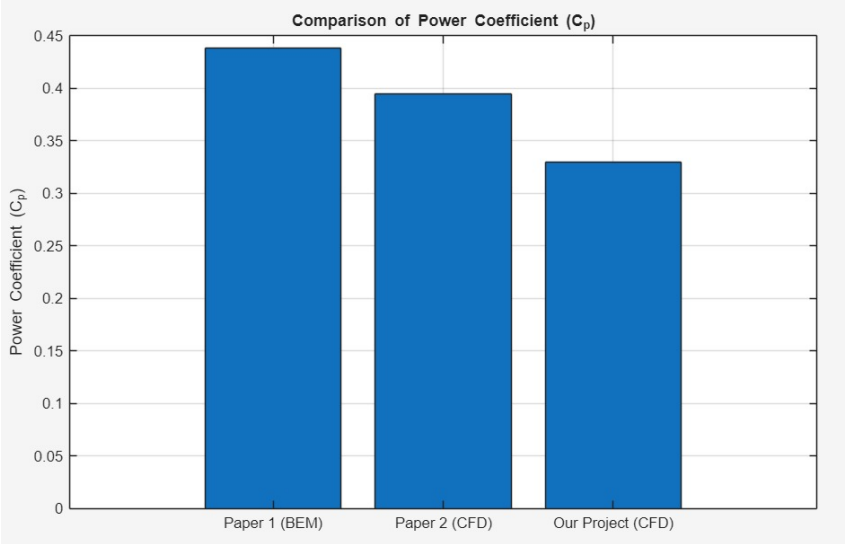


**Figure 35:** Comparison of power coefficient (Cp) between literature studies and our projec

## 9.3 Discussion of Differences

The variation in $C_p$ values is attributed to:

- **Operational Parameters:** The project used a fixed rotational speed (400 RPM) rather than a swept range of optimal Tip-Speed Ratios (TSR).
- **3D Effects:** CFD accounts for tip vortices, wake rotation, and turbulence, which are often neglected or simplified in analytical BEM.
- **Geometry:** Differences in hub treatment and blade span contribute to efficiency variations.

Despite these factors, the obtained coefficient lies within the realistic range for small-scale turbines, validating the physical accuracy of the simulation.

# 10 Conclusion

The comparison confirms that this project adheres to established aerodynamic design principles. The agreement in performance trends validates the CFD methodology, while the inclusion of structural integrity and resonance risk assessments provides a higher level of engineering significance than the reviewed literature.

# References

Radi, A., et al. (2024). *Metaheuristic optimization of wind turbine airfoils for enhanced aerodynamic performance*. Energies, 17(4), 1–18.

Terefa, T., et al. (2025). *Aerodynamic performance analysis of small-scale horizontal axis wind turbines using BEM, QBlade, and CFD*. Engineering, Technology & Applied Science Research, 15(1), 12345–12353.